FINITE DIFFERENCE MODELING OF WAVE PROPAGATION IN ACOUSTIC TILTED TI MEDIA

Linbin Zhang *

Earth Science Division, Lawrence Berkeley National Laboratory, Berkeley, CA94720, USA

James W. Rector III

Department of Civil and Environmental Engineering, University of California, Berkeley, CA94720, USA

G. Michael Hoversten

Earth Science Division, Lawrence Berkeley National Laboratory, Berkeley, CA94720, USA

*Formerly at Department of Material Science and Engineering, University of California, Berkeley, CA94720, USA

ABSTRACT

Based on an acoustic assumption (shear wave velocity is zero) and a dispersion relation, we derive an acoustic wave equation for P-waves in tilted transversely isotropic (TTI) media (transversely isotropic media with a tilted symmetry axis). This equation has fewer parameters than an elastic wave equation in TTI media and yields an accurate description of P-wave traveltimes and spreading-related attenuation. Our TTI acoustic wave equation is a fourth-order equation in time and space. We demonstrate that the acoustic approximation allows the presence of shear waves in the solution. The substantial differences in traveltime and amplitude between data created using VTI and TTI assumptions is illustrated in examples.

INTRODUCTION

There has been overwhelming seismological, structural and mineralogical evidence for extensive regions of elastic inhomogeneity and anisotropy within the Earth. Ignoring theses properties may lead to erroneous conclusions on the physical properties of the medium and therefore possibly poor geological interpretations. Hence the study of elastic wave propagation in inhomogeneous and anisotropic media is important in both global and exploration seismology.

To model seismic wave propagation in anisotropic media, one can solve the wave equation with numerical methods such as finite difference, finite element and pseudospectral methods (Igel, et al 1995; Carcione, 1999). To simulate P-waves propagation in vertical transversely isotropic (VTI) and orthorhombic anisotropic media, Alkhalifah (1998,2003) proposed an acoustic wave equation that was obtained by simply setting the vertical S-wave velocity to zero in the dispersion relation. This wave equation

reduces the computational costs because the P-wave propagation in VTI media can be modeled without solving the more complex anisotropic elastic wave equations. Alkhalifah (1998) showed that his acoustic VTI wave equation yields a kinematically accurate approximation of P-wave propagation.

The VTI assumption may not be routinely satisfied in the real world. For example, if the sedimentary layering is not horizontal, the symmetry axis of transverse isotropy is most likely tilted. In other words, a local symmetry assumption instead of a global one is more realistic. To study P-waves propagation in TTI media, we have modified Alkhalifah's VTI acoustic equation to incorporate a non-vertical, locally variable axis of symmetry. This allows the anisotropy to conform to spatially-variable structure.

In this paper we first obtain an expression for the phase velocity in TTI media. From the phase velocity we derive a dispersion relation and from the dispersion relation an acoustic wave equation is obtained. Finally we give some numerical examples to show the difference between VTI and TTI wavefields.

A TTI ACOUSTIC WAVE EQUATION

Consider a transversely isotropic medium with an axis of symmetry that is tilted by an angle, ϕ, from the vertical. We start with the VTI phase velocity expression (Tsvankin, 2001):

$$\frac{V^2(\theta)}{V_{P_0}^2} = 1 + \varepsilon \sin^2\theta - \frac{f}{2} \pm \frac{f}{2}\sqrt{(1 + \frac{2\varepsilon \sin^2\theta}{f})^2 - \frac{2(\varepsilon - \delta)\sin^2 2\theta}{f}} \quad , \qquad (1)$$

Rotating the symmetry axis from vertical to a tilt angle, ϕ, the phase velocity for P-waves is then rewritten as:

$$\frac{V^2(\theta,\phi)}{V_{P_0}^2} = 1 + \varepsilon \sin^2(\theta-\phi) - \frac{f}{2} \pm \frac{f}{2}\sqrt{(1+\frac{2\varepsilon\sin^2(\theta-\phi)}{f})^2 - \frac{2(\varepsilon-\delta)\sin^2(2(\theta-\phi))}{f}}, \quad (2)$$

where $f = 1 - \frac{V_{S0}^2}{V_{P0}^2}$. V_{P0} and V_{S0} are the quasi-P and quasi-S-wave velocity respectively. The variables ε and δ are Thomsen parameters (Thomsen, 1986) and are defined as:

$$\varepsilon = \frac{c_{11}-c_{33}}{2c_{33}} \quad ; \qquad \delta = \frac{(c_{13}+c_{44})^2 - (c_{33}-c_{44})^2}{2c_{33}(c_{33}-c_{44})} \quad , \qquad (3)$$

In Eq.(1), the positive sign in front the radical is the quasi-P-wave and negative sign is the quasi-S-wave.

For plane wave propagation, we have:

$$\sin\theta = \frac{V(\theta,\phi)k_x}{\omega} \quad , \cos\theta = \frac{V(\theta,\phi)k_z}{\omega}, \qquad (4)$$

where k_x and k_z are the wavenumbers in x- and z- directions, respectively. ω is the temporal frequency. To model P-wave propagationin VTI media ($\phi = 0$), Alkhalifah (1998) simply set V_{S0}=0 since V_{S0} has very little influence on P-wave phase and group velocities (Alkhalifah, 1998,2003; Stopin, 2000). The resulting equation obtained by Alkhalifah is:

$$\frac{\partial^2 P}{\partial t^2} = (1+2\eta)V_{NMO}^2\frac{\partial^2 P}{\partial x^2} + V_{P0}^2\frac{\partial^2 P}{\partial z^2} - 2\eta V_{NMO}^2 V_{P0}^2\frac{\partial^4 F}{\partial x^2 \partial z^2},$$

$$P = \frac{\partial^2 F}{\partial t^2}, \qquad (5)$$

To incorporate tilt, we combine Eq.(2) and (4) to obtain:

$$a_4 k_z^4 + a_3 k_z^3 + a_2 k_z^2 + a_1 k_z + a_0 = 0 , \qquad (6)$$

where

$$a_4 = \frac{1}{2}(\varepsilon - \delta)\sin^2 2\phi ,$$

$$a_3 = -(\varepsilon - \delta)\sin 4\phi k_x ,$$

$$a_2 = [-(\varepsilon - \delta)\sin^2 2\phi + 2(\varepsilon - \delta)\cos^2 2\phi]k_x^2 - (1 + 2\varepsilon\sin^2\phi)\omega^2 / V_{P_0}^2 ,$$

$$a_1 = (\varepsilon - \delta)\sin 4\phi k_x^3 + \frac{2\varepsilon\omega^2}{V_{P_0}^2}\sin 2\phi k_x ,$$

$$a_0 = \frac{1}{2}(\varepsilon - \delta)\sin^2 2\phi k_x^4 - (1 + 2\varepsilon\cos^2\phi)k_x^2\omega^2 / V_{P_0}^2 + \frac{\omega^4}{V_{P_0}^4} ,$$

Multiplying both sides of Eq.(5) with the wavefield in the Fourier domain, $F(k_x, k_z, \omega)$, and applying an inverse Fourier transform in k_x, k_z and ω, ($kl \to -i\frac{\partial}{\partial l}, \omega \to i\frac{\partial}{\partial t}$, $l = x, z$), we obtain:

$$\frac{\partial^2 P}{\partial t^2} = (V_{P0}^2 \sin^2\phi + {V_{NMO}}^2(1 + 2\eta)\cos^2\phi)\frac{\partial^2 P}{\partial^2 x} + (V_{P0}^2 \cos^2\phi + {V_{NMO}}^2(1 + 2\eta)\sin^2\phi)\frac{\partial^2 P}{\partial^2 z}$$
$$+ (V_{P0}^2 - {V_{NMO}}^2(1 + 2\eta))\sin 2\phi \frac{\partial^2 P}{\partial x \partial z} - V_{P0}^2 {V_{NMO}}^2 \eta(2 - 3\sin^2 2\phi)\frac{\partial^4 F}{\partial x^2 \partial z^2} - \frac{1}{2}V_{P0}^2 {V_{NMO}}^2 \eta \sin^2 2\phi \frac{\partial^4 F}{\partial z^4}$$
$$+ V_{P0}^2 {V_{NMO}}^2 \eta \sin 4\phi \frac{\partial^4 F}{\partial x \partial z^3} - V_{P0}^2 {V_{NMO}}^2 \eta \sin 4\phi \frac{\partial^4 F}{\partial x^3 \partial z} - \frac{1}{2}V_{P0}^2 {V_{NMO}}^2 \eta \sin^2 2\phi \frac{\partial^4 F}{\partial x^4}$$

, (7)

where:

$$P = \frac{\partial^2 F}{\partial t^2}, \tag{8}$$

$$V_{NMO} = V_{P0}\sqrt{1+2\delta}, \quad \eta = \frac{\varepsilon - \delta}{1+2\delta},$$

V_{NMO} is the NMO velocity.

This equation is a fourth-order partial differential equation in t, x and z. For the compressional-wave, we interpret the wavefield P as pressure or as a scalar potential. When η=0 and $V_{NMO} = V_{P0}$ Eq.(6) becomes the standard acoustic wave equation for isotropic media. When ϕ=0, Alkhalifah's VTI acoustic wave equation Eq. (5) is obtained. Eq.(7) has two sets of complex conjugate solutions. One set will grow exponentially when η < 0 (Klie, Toro, 2001; Grechka et al, 2004), hence causing serious stability problems. Thus this TTI wave equation can be only used when $\eta \geq 0$. Fortunately, most η values corresponding to anisotropies in the subsurface are likely to have positive values.

In this study, we use a high-order, explicit finite difference scheme to solve Eq.(7) and (8). Instead of using Taylor expansion to obtain finite difference coefficients we calculate the finite difference coefficients in the wavenumber domain (see Appendix A). With these coefficients a coarser grid can be used resulting in memory and computational time savings. At the top of the model one can use the free-surface boundary or absorbing boundary conditions. Absorbing boundary conditions are applied on the other three boundaries of the model (Cerjan, et al, 1985). The computational procedure is to define

the tilt angle,η, V_{NMO} and V_{P0} at each grid point then to solve Eq. (7) and (8) with the finite difference scheme for as many time steps as needed.

NUMERICAL EXAMPLES

CAN SHEAR WAVES BE OBSERVED IN DATA MODELED BY THIS 'ACOUSTIC' TI WAVE EQUATION

The first example is a homogeneous tilted TI model with $Vp_0 = 2500$ m/s, $Vs_0 = 1500$ m/s, $\delta = 0.1$, $\varepsilon = 0.25$, $\eta = 0.125$, $\gamma = 0.1$ and a tilt angle $\phi=30^0$. Figure 1 (a) shows a snapshot of the normal stresses (z-component) at 0.3 s obtained with the elastic wave equation. Figure 1(b) is a pressure snapshot generated by our acoustic wave equation at 0.3s. For the P wave, the acoustic and the elastic wavefields are kinematically similar. Dynamically, they differ considerably. Both wavefields have a secondary arrival. The elastic wavefield secondary arrival is an S wave. The comparable wavefront in the acoustic wavefields is the diamond-shaped wavefront (Figure 1). This diamond-shaped wavefront from the TTI acoustic wave equation is a quasi-S-wave wavefront (Grechka, et al 2004).

To numerically demonstrate that the diamond-shaped wavefront is an S-wave wavefront, we calculate the group velocities of the P- and S-waves by using Eq. (2) and compute P- and S-wave wavefronts. Figure 2 shows the wavefronts overlaid on a snapshot obtained by wave Eq. (6) and (7) with V_{NMO}=Vp0=2000m/s, η=0.4 and tilt angle ϕ=0 (VTI). They match very well. This result clearly shows that the diamond-shaped wavefront is a S-wave wavefront. This S-wave has lower velocity than the P-wave. As a result, high accuracy numerical methods such as high-order finite difference scheme (FD) or pseudo-spectral methods (PS) may be needed to insure stability at a

selected grid spacing. Figure 3(a) and 3(b) show the snapshots at 0.14 s generated by the 4^{th}-order FD and PS methods, respectively. The velocity model is a homogeneous TTI model with $Vp_0 = 2500$ m/s, $Vnmo = 2738.6$ m/s , $\eta = 0.125$ and a tilt angle ϕ=42^0. We used a large tilt angle, because the group velocity is lowest at 45 degrees and requires more numerical accuracy for a given grid spacing. With the 4^{th}-order FD the simulation begins to become unstable after 700 time steps, whereas the PS solution does not exhibit any instability.

One possible approach for removing shear-waves is to make the weak anisotropy approximation (Appendix B).

THE EFFECT OF TILT ON TRAVELTIMES

Figure 4 shows wavefield snapshots for four different tilt angles and Figure 5 shows the common shot gathers corresponding to these different tilt angles. The model is homogenous with $V = V_{P0} = 2000$ m/s and η=0.4. It can be seen that a tilted axis of symmetry has a significant effect on the traveltimes and moveouts. For example, the traveltime difference between zero tilt (Figure 5 (b)) and a tilt angle of 60 degrees (Figure 5 (d)) is bigger than100 ms, which corresponds to 1.5 wavelength. Therefore a tilted axis of symmetry will obviously affect both the positioning and focusing of events in seismic migration.

A more realistic velocity model, taken from a real-world offshore prospect, is shown in Figure 6. The parameters ε and δ are zero in the water layer and linearly increase from 0 at the sea floor to $\varepsilon = 0.25$ and $\delta = 0.05$ at the first sub-seafloor horizon. Below the first sub-seafloor horizon ε and δ are constant with ε=0.25 and δ=0.05. Synthetic shot records (Figure 7) were calculated using the 4^{th} order optimized coefficient FD method

applied to Eq.(5) with absorbing boundaries. In this common shot gather it is hard to see the S-wave because we placed the source in the water which is a isotropic medium. The shot records clearly shows how events are shifted both vertically and laterally when tilt angle is considered. The moveout difference of the reflection at 5 seconds between VTI and TTI is approximately 0.2s. The reflections at 5 seconds and between 3.5 and 4 seconds (indicated by arrows) have large amplitudes in the TTI shot records, and low amplitudes in VTI shot record. These amplitude differences are due mainly to geometrical spreading as well as reflectivity. Though the acoustic equation does not provide accurate reflection and transmission coefficients for the elastic wave, it provides correct simulation of the geometrical spreading behavior of the waves, which directly affect the amplitudes. Such differences in travel times as well as amplitudes will considerably hamper VTI processing when tilt angles are ignored.

CONCLUSIONS

We have formulated and implemented a new acoustic wave equation for modeling P-wave propagation in tilted transversely isotropic media. With the acoustic wave equation the anisotropy conform to spatially-variable structure which allows us to model P-wave propagations in more realistic Earth structures.

Numerical examples show that this new acoustic equation yields good kinematic P-wave approximations to the elastic wave equation. The acoustic wave equation is not only computationally efficiency because we can model the P-wave propagation in TTI media without solving the more complex anisotropic elastic wave equations, but also convenient for generating migration and inverse algorithms, such as those used in reverse-time migration. Although we have claimed an ‘acoustic‘ wave equation, S-waves

still exists in VTI and TTI acoustic wave equation. Because the S-waves in the acoustic wave equation have low velocity, a highly accurate numerical method such as high-order FD is required in order to reduce dispersion and to avoid instability. To generate pure P-waves in weakly anisotropic media, we derive an approximation free of S-waves.

One very practical conclusion in the examples is that the differences between VTI and TTI wavefields are a direct indication of the magnitude and traveltime of errors incurred if a VTI interpretation is performed when TTI is present. In other word, ignoring tilt angle may introduce significant errors on anisotropic parameter estimation and migration.

ACKNOWLEGMENTS

We thank Vladimir Grechka and anonymous reviewers for constructive comments that improved the manuscript. Support for this work was provided by the Assistant Secretary for Fossil Energy and through the National Energy Technology Laboratory under U.S. Department of Energy under Contract No. DE-AC03-76SF00098.

REFERENCES

Alkhalifah, T., 2003, An acoustic wave equation for orthorhombic anisotropy: Geophysics, **68**, 1169-1172.

Alkhalifah, T., 1998, An acoustic wave equation for anisotropic media., 68th Annual Internat. Mtg., Soc. Expl. Geophys., Expanded Abstracts, 1913-1916.

Alkhalifah, T., 1998, Acoustic approximations for processing in transversely isotropic media: Geophysics, **63**,623-631.

Carcione, J. M., 1999, Staggered mesh for the anisotropic and viscoelastic wave equation: Geophysics, **64,** 1863-1866.

Cerjan, C., Kosloff, D., Kosloff, R., and Reshef, M., 1985, A nonreflecting boundary condition for discrete acoustic and elastic wave equations, Geophysics, **60**,705-708.

Dellinger, J., and Etgen, J., 1990, Wavefield separation in 2-D anisotropic media: Geophysics, **55**,914-919.

Gazdag, J., 1981, Modeling of the acoustic wave equation with transform method, Geophysics, **46**,854-859.

Grechka, V., Zhang, L. and Rector, J.W., 2004, Shear waves in acoustic anisotropic media, Geophysics, **69**,576-582.

Igel, H., Mora, P., and Riollet, B., 1995, Anisotropic wave propagation through finite-difference grids, Geophysics, **53**, 1045-1055.

Klie, H. and Toro,W., 2001, A new acoustic wave equation for modeling in anisotropic media: 71th Annual Internat. Mtg., Soc. Expl. Geophys., Expanded Abstracts,1171-1174.

Rector, J.W., Zhang, L.B. and Hoversten, G.M., 2002, Optimized Coefficient Finite Difference Scheme For Wave Equation, forward modeling workshop, 72th Annual Internat. Mtg., Soc. Expl. Geophys. Salt Lake City, UT.

Stopin, A., 2000, comparison of v(theta) equations in TI media: 9th International Workshop on Seismic Anisotropy.

Thomsen, L., 1986, Weak elastic anisotropy, Geophysics, **51**, 1954-1966.

Tsvankin, I., 2001, Seismic signatures and analysis of reflection data in anisotropic media: Elsevier Science Publ.. Co., Inc.

APPENDIX A

Numerical Solutions of the wave equation

Eq. (4) and (5) can be solved numerically, such as by finite-difference or pseudo-spectral methods (PS). In pseudo-spectral method the spatial derivatives of a function $g(x,z)$ can calculated by the discrete Fourier transform:

$$\frac{\partial^{m+n} g(x,z)}{\partial^m x \partial^n z} = DFT^{-1}((-ik_x)^m (-ik_z)^n DFT(g(x,z))), \qquad \text{(A1)}$$

where $x = j\Delta x, j = 0,1,...,N-1$, $z = j\Delta z, j = 0,1,...,M-1$, Δx and Δz are the sampling interval in x and z direction, respectively. k_x and k_z are discrete variables given by:

$$k_x = \frac{2\pi j}{N\Delta x}, \qquad k_z = \frac{2\pi k}{M\Delta z} \quad ,$$

where j and k are integer number.

In the finite difference method, the m-th derivative of the $g(x)$ may be approximated by the 2N-th order finite difference scheme:

$$\frac{\partial^m g(x)}{\partial x^m} \approx \frac{1}{\Delta x^m}[g(x)a_0 + \sum_{j=1}^{N} a_j (g(x + j\Delta x) + (-1)^m g(x - j\Delta x))] \ , \qquad \text{(A2)}$$

where $a_j, j = 0,1,2...,N$, are the coefficients to be determined, and a_0 =0 if m is an odd number.

Taking Fourier transform of Eq.(A2):

$$(ik)^m g(x) \approx \frac{1}{\Delta x^m}[a_0 + \sum_{j=1}^{N} a_j (e^{ijk\Delta x} + (-1)^m e^{-ijk\Delta x})]g(x) \ ,$$

where $i = \sqrt{-1}$. The coefficients $a_j, j = 0,1,2...N$, can be computed to minimize a least-squares function:

$$E(a_j) = \int_0^{K_{\max}} [(iK)^m - (a_0 + \sum_{j=1}^{N} a_j (e^{ijK} + (-1)^m e^{-ijK})]^2 W(K) d_K \ , \quad \text{(A3)}$$

where $K = k\Delta x$. The weight function $W(K)$ may be selected to emphasize a specific wavenumber. Solving the discrete form of Eq. (A3) via singular valued decomposition, we can obtain the coefficients $a_j, j = 0,1,2...N$. For mixed derivatives, we calculate one direction first then do the other direction.

The second finite-difference approach was employed to the temporal derivatives:

$$\frac{\partial^2 P(t)}{\partial t^2} = \frac{P(t+\Delta t) - 2P(t) + P(t-\Delta t)}{\Delta t^2}, \qquad \text{(A4)}$$

$$P(t) = \frac{F(t+\Delta t) - 2F(t) + F(t-\Delta t)}{\Delta t^2}, \qquad \text{(A5)}$$

Higher-order finite-difference approximations with the optimized coefficients (Rector, et al, 2002) can also be used to solve Eq. (4) and (5) directly. In order to avoid numerical dispersion and instability, we use the same constrains and rules used in the isotropic case. The spacing Δx and Δz should satisfy:

$$\max(\Delta x, \Delta z) \le \frac{V_{\min}}{\vartheta f_{\max}}, \qquad \text{(A6)}$$

and the stability condition :

$$\Delta t \le \frac{\gamma \min(\Delta x, \Delta z)}{V_{\max}}, \qquad \text{(A7)}$$

where ϑ is the number of samples per minimum wavelength, and $V_{\min}$ and $V_{\max}$ are the minimum and maximum velocities, respectively. γ is a constant. In the isotropic case, $\gamma = \frac{1}{\sqrt{2}}$ and $\gamma = \sqrt{\frac{3}{8}}$ for the 2nd and 4th order conventional FD scheme, respectively.

APPENDIX B

A TTI acoustic wave equation in weak anisotropic media

In weak anisotropic media, using a weak anisotropy squared approximation, Eq. (1) can be written as:

$$V_P^2(\theta,\phi) = V_{P0}^2(1 + 2\delta \sin^2(\theta-\phi)\cos^2(\theta-\phi) + 2\varepsilon \sin^4(\theta-\phi)),$$

The P-wave TTI acoustic wave equation in weak anisotropic media becomes:

$$\frac{\partial^2 F(k_x,k_z,t)}{\partial t^2} = V_{P0}^2[k_x^2 + k_z^2 + (2\delta\sin^2\phi\cos^2\phi + 2\varepsilon\cos^4\phi)\frac{k_x^4}{k_x^2+k_z^2} + (2\delta\sin^2\phi\cos^2\phi + 2\varepsilon\sin^4\phi)\frac{k_z^4}{k_x^2+k_z^2}$$

$$+ (-\delta\sin^2 2\phi + 3\varepsilon\sin^2 2\phi + 2\delta\cos^2 2\phi)\frac{k_x^2 k_z^2}{k_x^2+k_z^2} + (\delta\sin 4\phi - 4\varepsilon\sin 2\phi\cos^2\phi)\frac{k_x^3 k_z}{k_x^2+k_z^2}$$

$$+ (-\delta\sin 4\phi - 4\varepsilon\sin 2\phi\sin^2\phi)\frac{k_x k_z^3}{k_x^2+k_z^2}]F(k_x,k_z,t) \quad , \quad \text{(B)}$$

The four snapshots with wave Eq. (B) are shown in Figure A. There is no S-wave in these snapshots.

FIGURES

Figure 1. Snapshots for elastic wavefield and TTI acoustic equation at 0.3 s. $Vp_0 = 2500$ m/s , $Vs_0 = 1500$ m/s, $\delta = 0.1$, $\varepsilon = 0.25$, $\eta = 0.125$, $\gamma = 0.1$ and a tilt angle $\phi=30^0$. (a) the z-component of normal stresses. (b) compressional wavefield.

Figure 2. Wavefronts (red solid lines) at 0.375s obtained from P- and S-wave group velocities superimposed on snapshot calculated by acoustic wave equation (5). V=Vp0=2000m/s. The source is in the model center, η =0.4 and ϕ=0.

Figure 3. Snapshot generated with the 4th-order FD at 0.14 s. The velocity model is a homogeneous TTI model with $Vp_0 = 2500$ m/s, $Vnmo = 2738.6$ m/s , $\eta = 0.125$ and a tilt angle $\phi=42^0$.

Figure 4. Snapshot generated with pseudo-spectral method at 0.14 s. The velocity model is the same as that in Figure 3. No dispersion can be seen in this result.

Figure 5. Snapshots for TTI acoustic wave equation. V=Vp0=2000m/s. The source is in the model center. (a)η =0. Isotropic media. (b)η =0.4 and ϕ=0. VTI model. (c) η =0.4 and $\phi=30^0$, (d) η =0.4 and $\phi=60^0$.

Figure 6. Common shot gathers in Fig.2 models. The source is in the model center and receivers are on the top boundary. (a) isotropic, (b) VTI, (c) TTI, $\phi=30^0$, (d)TTI, $\phi=60^0$. The traveltime differences between VTI and TTI are only attributed to tilt angles.

Figure 7. From top to bottom: vertical velocity, tilt angle.

Figure 8. VTI seismogram (top) and TTI seismogram (bottom). The arrows point to some of differences in energy and arrival times between VTI and TTI. The differences of traveltime and amplitude between VTI and TTI are only attributed to tilt angles.

Figure A. Snapshots generated by equation (A) at 0.3 s with tilt angle 0 , 30^0 ,60^0 and 90^0, respectively. The S-wave does not exist in wave equation (B).

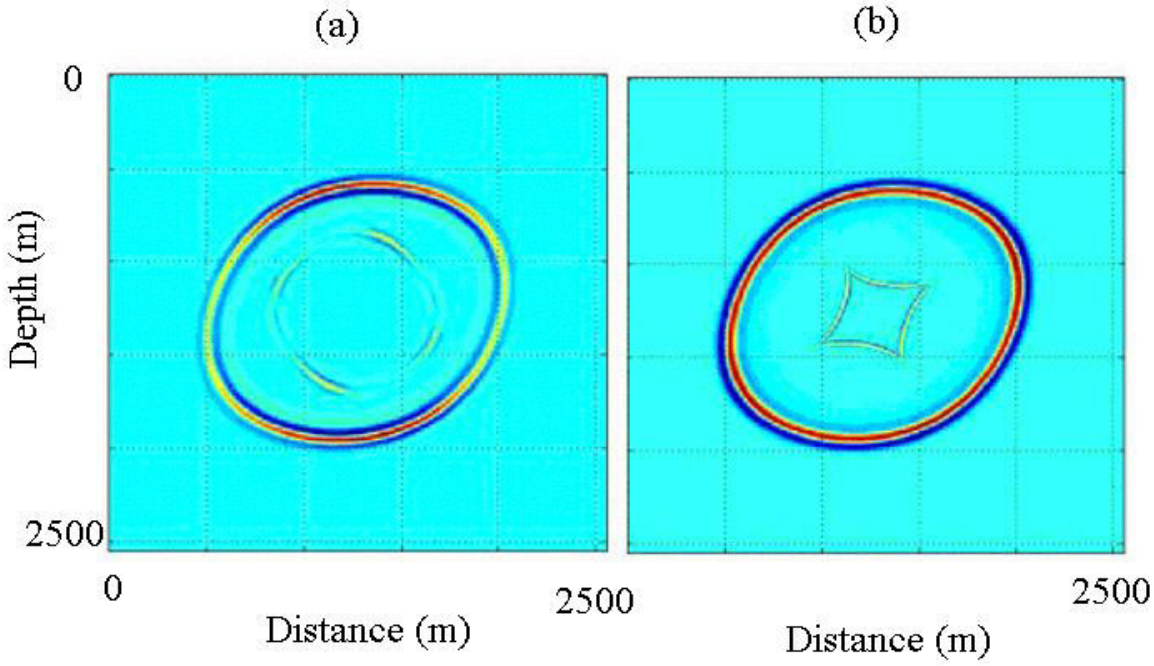

Figure 1. Snapshots for (a) the z-component of normal stresses elastic wavefield and (b) compressional wavefield TTI acoustic equation at 0.3 s. $Vp_0 = 2500$ m/s , $Vs_0 = 1500$ m/s, $\delta = 0.1$, $\varepsilon = 0.25$, $\eta = 0.125$, $\gamma = 0.1$ and a tilt angle ϕ=30^0.

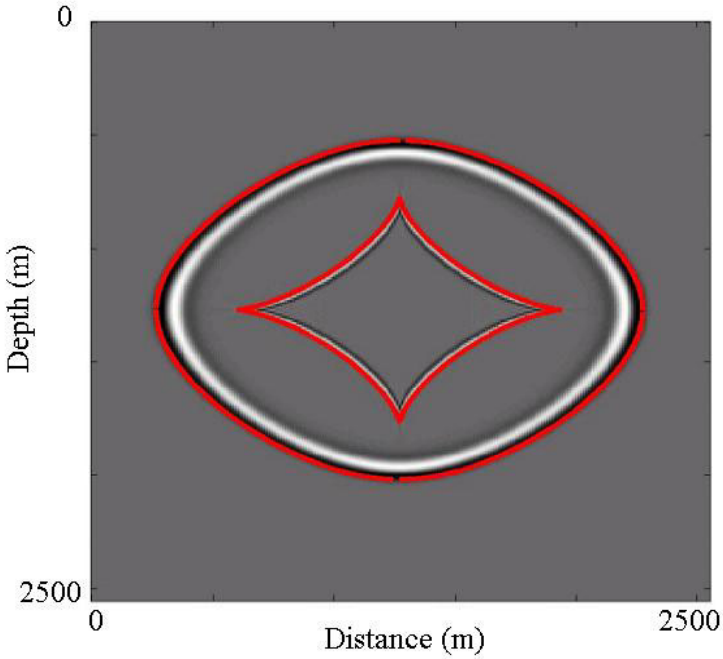

Figure 2. Wavefronts (red solid lines) at 0.375s obtained from P- and S-wave group velocities superimposed on snapshot calculated by acoustic wave equation (5). V=Vp0=2000m/s. The source is in the model center, η =0.4 and ϕ=0.

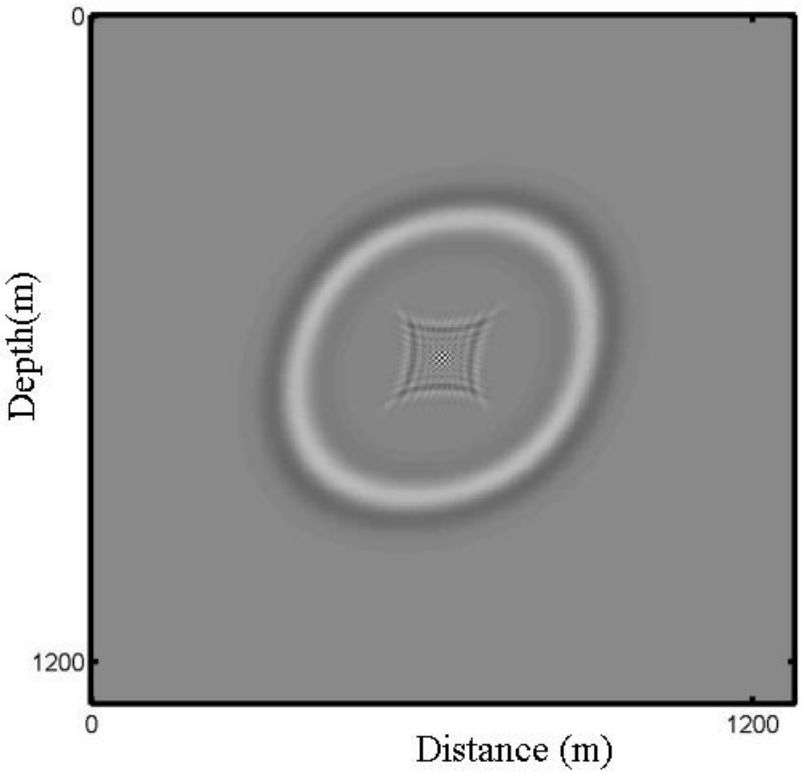

Figure 3. (a)

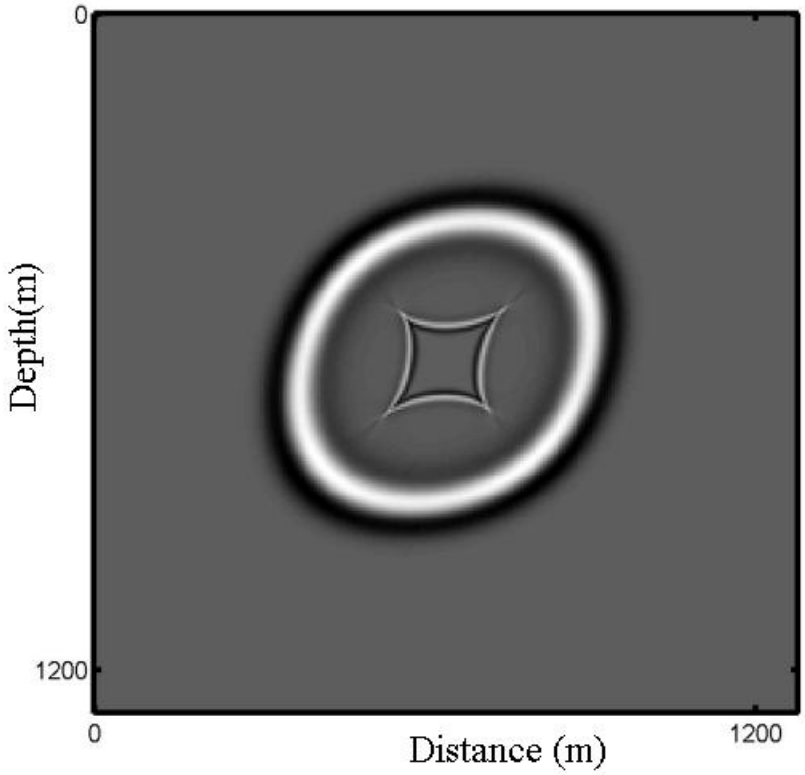

Figure 3(b)

Figure 3. Snapshot generated with (a) the 4th-order FD and (b) pseudo-spectral method at 0.14 s. The velocity model is a homogeneous TTI model with $Vp_0 = 2500$ m/s, $Vnmo = 2738.6$ m/s , $\eta = 0.125$ and a tilt angle ϕ=42^0.

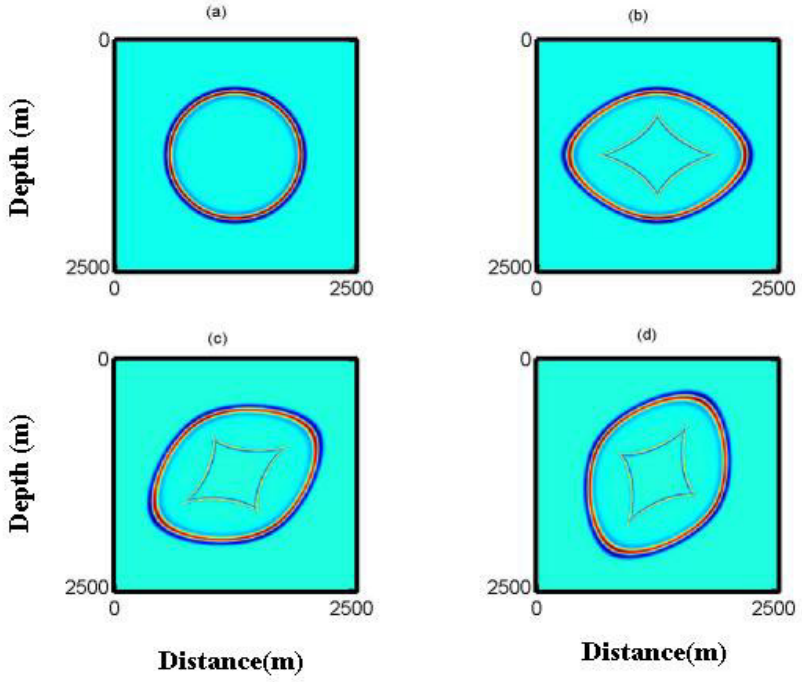

Figure 4. Snapshots for the TTI acoustic wave equation. V=Vp0=2000m/s. The source is in the model center. (a)η =0. Isotropic media. (b)η =0.4 and ϕ=0. VTI model. (c) η =0.4 and $\phi=30^0$, (d) η =0.4 and $\phi=60^0$.

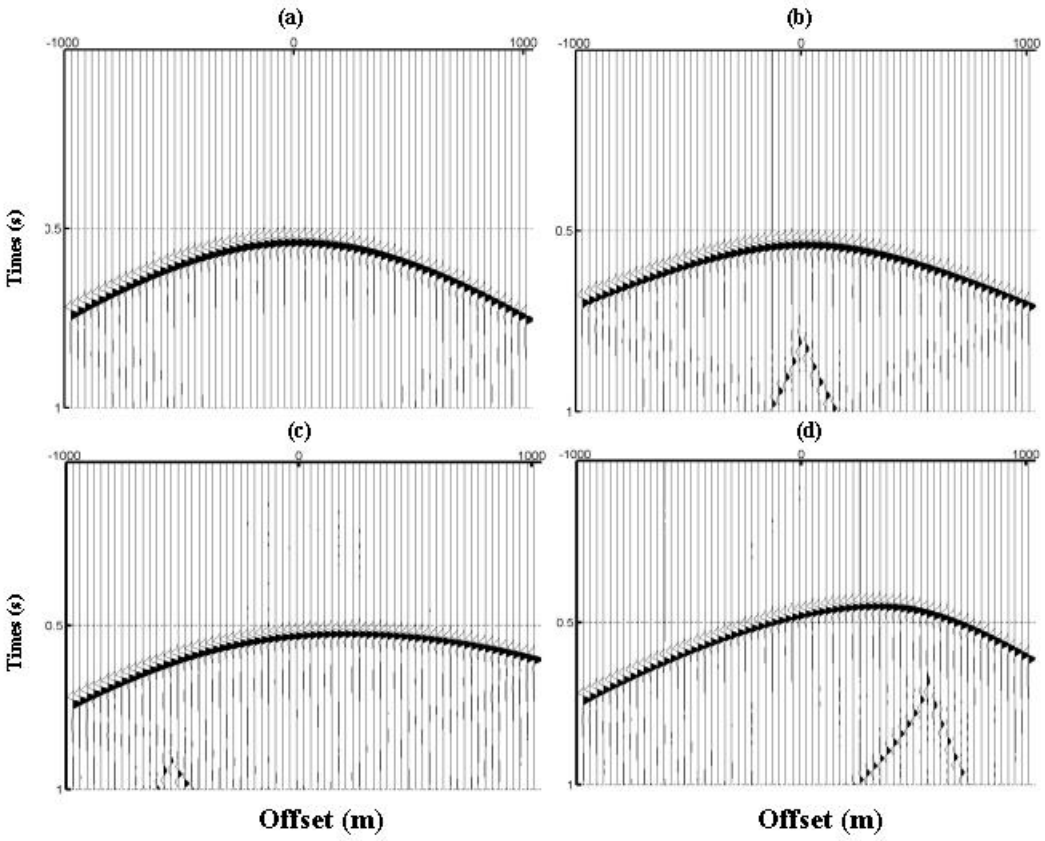

Figure 5. Common shot gathers corresponding to the model shown in Fig.2 models. The source is in the model center and receivers are on the top boundary. (a) isotropic, (b) VTI; (c) TTI, $\phi=30^0$; (d)TTI, $\phi=60^0$. The traveltime differences between VTI and TTI are only attributed to tilt angles.

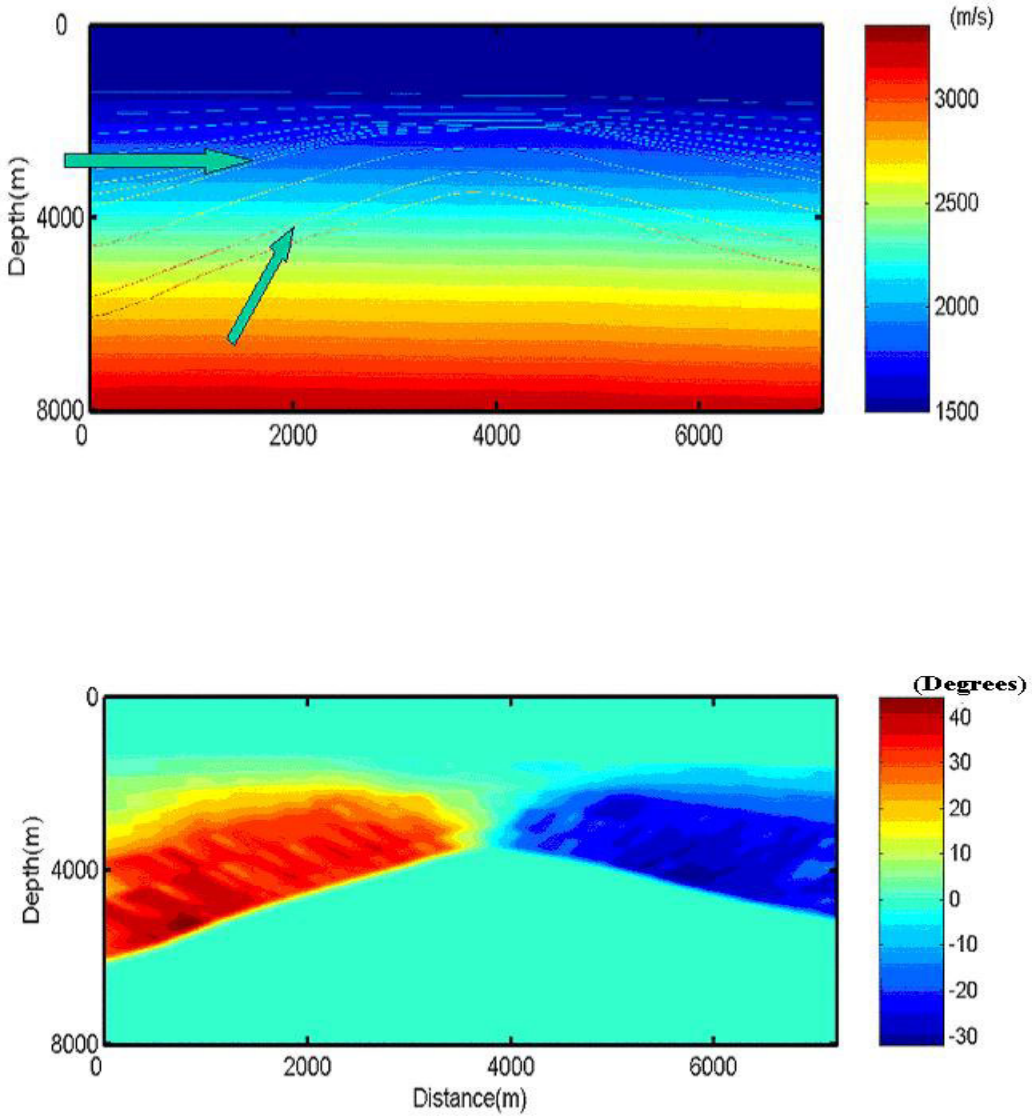

Figure 6. From top to bottom: vertical velocity, tilt angle.

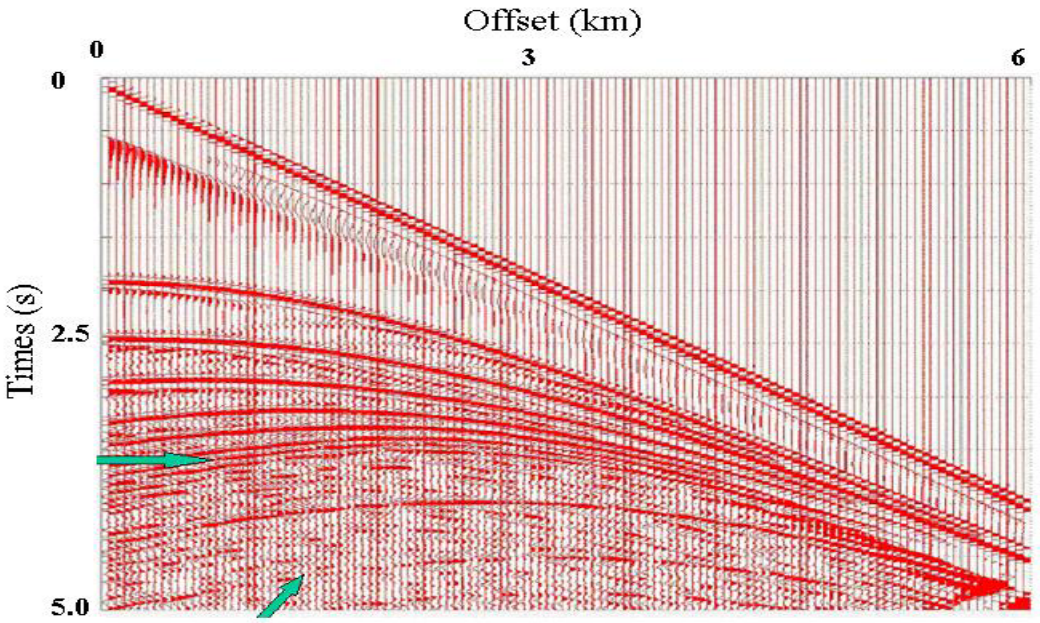
Offset (km)
0
3
6
0
2.5
5.0
Times (s)

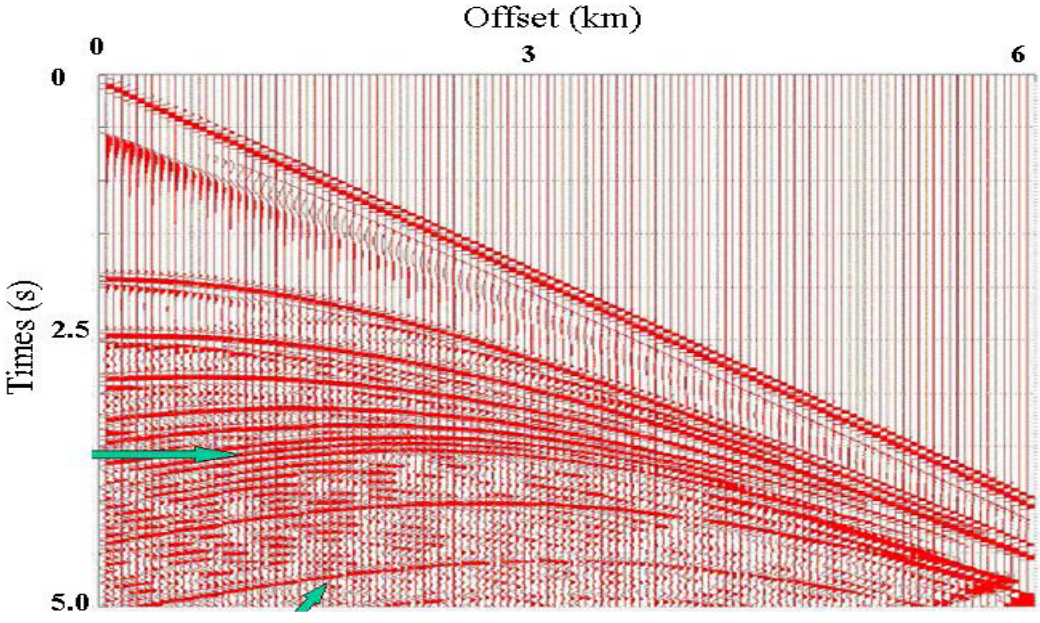
Offset (km)
0
3
6
0
2.5
5.0
Times (s)

Figure 7. VTI seismogram (top) and TTI seismogram (bottom). The arrows point to some of differences in energy and arrival times between VTI and TTI. The differences of traveltime and amplitude between VTI and TTI are only attributed to tilt angles.

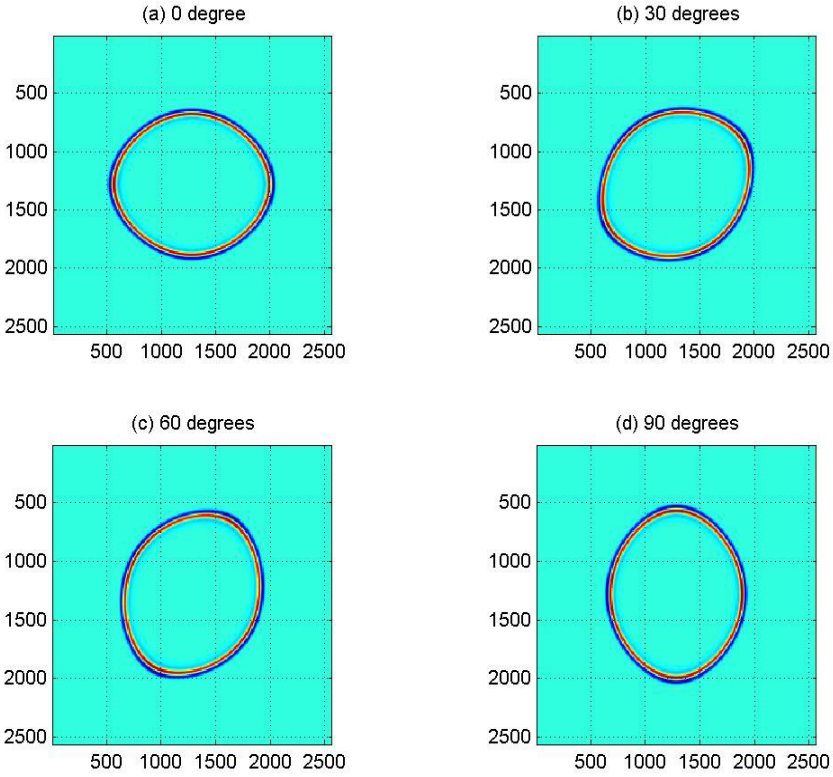

Figure A. Snapshots generated by equation (B) at 0.3 s with tilt angle 0, 30^0,60^0 and 90^0, respectively. The S-wave does not exist in wave equation (B).